RSC Advances

PAPER

View Article Online
View Journal | View Issue

Cite this: *RSC Adv.*, 2019, **9**, 8600

Novel cathepsin K inhibitors block osteoclasts *in vitro* and increase spinal bone density in zebrafish†

Si-tu Xue,‡ Ya-li Wang,‡ Xiao-wan Han, Hong Yi, Wei Jiang, Shu-yi Si, Hui-fang Guo* and Zhuo-rong Li *

Cathepsin K (Cat K) is a predominant cysteine protease and highly potent collagenase expressed in osteoclasts. Cat K inhibitors are anti-resorptive agents to treat osteoporosis. A novel scaffold of cathepsin K inhibitors, exemplified by lead compound **1x**, was used as the template for designing and synthesizing a total of 61 derivatives that have not been reported before. An exploratory structure–activity relationship analysis identified the potent Cat K inhibitor **A22**, which displayed an IC_{50} value of 0.44 μM against Cat K. **A22** was very specific for Cat K and caused a significantly higher *in vitro* inhibition of the enzyme as compared to that of lead compound **1x**. A surface plasmon resonance analysis confirmed *in vitro* binding of **A22** to Cat K. Molecular docking studies indicated several favourable interaction sites for **A22** within the active pocket of Cat K. Furthermore, **A22** also blocked active osteoclasts *in vitro* and increased spinal bone density in zebrafish, in which it showed an activity that was higher than that of the marketed therapeutic bone metabolizer etidronate disodium. **A22** represents a very promising lead compound for the development of novel antiresorptive agents functioning as orthosteric inhibitors of Cat K.

Received 17th December 2018
Accepted 26th February 2019

DOI: 10.1039/c8ra10338k

rsc.li/rsc-advances

1. Introduction

Osteoporosis (OP) is a systemic disease associated with a declining rigidity and mechanical stability of the bones.[1] Current estimates indicate that over 200 million people worldwide suffer from this disease, causing more than 8.9 million fractures annually. In fact, an osteoporotic fracture is estimated to occur every 3 s, and one out of every three women and one in five men over 50 years of age will have an OP-related fracture in their lifetime.[2,3] A better knowledge about the progression of bone metabolic disorder and the development of effective treatments will have important socio-economic and medical consequences. The most commonly prescribed OP medications include nitrogen-containing bisphosphonates, denosumab, raloxifene, hormone replacement therapy, and calcitonin.[4] Although these therapies improve the quality of life in patients with OP, they have many side effects.[5–7] Thus, the discovery of novel OP medications is a priority that would provide new options for OP patients and represent a major advancement in the treatment of OP.

Bone health in adults depends on resorption that involves the continuous removal of old or damaged bone tissue by osteoclast (OC) cells, which is balanced by the deposition of new bone formed by osteoblast (OB) cells. As the skeleton ages, the action of the OCs outpaces that of the OBs, causing a shift toward excessive resorption and the development of chronic OP associated with reduced bone mineral density (BMD) and an increased risk of bone fractures.[8,9] Cathepsin K (Cat K) is a lysosomal cysteine protease released by OCs, which cleaves the collagen matrix of bone tissue.[10,11] Cat K knockout mice have been shown to develop osteopetrosis with elongated bones and vertebrae and abnormal joint morphology due to a deficit in matrix degradation,[12] indicating the potential role of Cat K in OP and other bone diseases. In recent years, Cat K inhibitors have been intensively studied by pharmaceutical companies to find antiresorptive therapies for OP.[13–15] The most advanced drug candidates include odanacatib,[16,17] relacatib,[18,19] balicatib[20,21] and ONO-5334 (Fig. 1).[22,23] Odanacatib and balicatib are

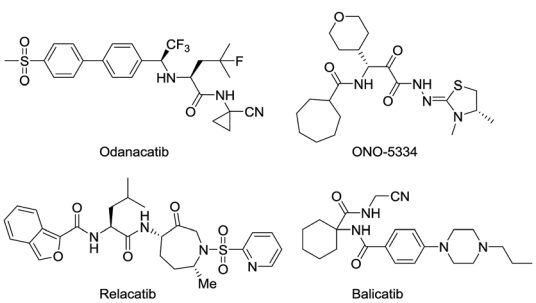

Fig. 1 Structures of Cat K inhibitors.

Institute of Medicinal Biotechnology, Chinese Academy of Medical Science and Peking Union Medical College, Beijing 100050, China. E-mail: lizhuorong@imb.pumc.edu.cn; huifangguo@imb.pumc.edu.cn

† Electronic supplementary information (ESI) available. See DOI: 10.1039/c8ra10338k

‡ The authors contribute equally to this work.

reversible covalent Cat K inhibitors carrying a cyano group that can form a covalent bond with C25 of the active pocket in Cat K.

Odanacatib was once the most advanced drug candidate as a Cat K inhibitor that reduced fractures in postmenopausal women in a large multinational randomized, double-blinded phase III clinical study. However, odanicatib was also associated with an increased risk of cerebrovascular accidents and subsequently withdrawn from the regulatory approval process.

Thus, there is significant value in the study of Cat K because it is a major drug target for OP and related-bone disorders.

Our research team has been working on the development of anti-OP drugs for many years.[24,25] Our recent efforts are focused on the discovery of Cat K inhibitors as potent antiresorptive agents. A virtual screen of our in-house compound library against the Cat K (PDB code: 4dmy, Fig. 2) active site identified compound **1q** (Fig. 2). **1q** had a higher CDOCKER score than the covalent Cat K inhibitor **14** which was reported by Alexander G. Dossetter and his colleagues (Fig. 2a).[26] The orientation of **1q** also showed a high fitness comparable to that of **14** (Fig. 2b). The scaffold of **1q** has not been reported by others as a Cat K inhibitor. A search of our in-house compound library identified several structural analogues of **1q** that were all tested for *in vitro* Cat K inhibiting effects using an enzymatic assay. However, **1q** was not active against Cat K at 100 μM. Interestingly, we identified compound **1x** (Fig. 2) with a scaffold of benzimidazole-2-substituted pyridine propyl ketene that inhibited Cat K at a concentration below 100 μM. Two other compounds (Fig. 3, **1o** and **1p**[27]) with a scaffold containing benzoxazole or benzothiazole did not inhibit Cat K. We also found that the carbonyl group in **1x** scaffold is probably essential for the Cat K inhibiting activity because the switch to a hydroxyl group (see **1s** and **1t**[27] in Fig. 3) abolished the activity.

The IC_{50} of compounds **1o**, **1p**, **1s**, and **1t** against Cat K were all above 100 μM.

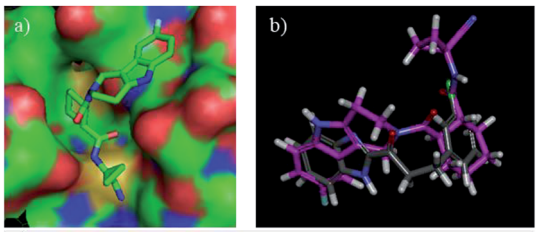

	–CDOCKER ENERGY	Cat K IC_{50} (μM)
14	21.3069	< 0.001
1q	23.1731	> 100
1x	14.7498	10.04

Fig. 2 Virtual screen found Cat K inhibitor **1x**. (a) The 3D model of Cat K inhibitor **14** in docking position (PDB code 4dmy; the picture was prepared with Pymol) in the active site of Cat K and (b) comparison of the docking position of **1q** (grey) with **14** (purple) and (c) structures, CDOCKER scores and Cat K IC_{50}s of **14**, **1q** and **1x**.

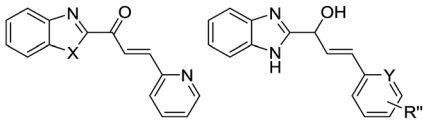

Fig. 3 Inactive compounds against Cat K.

In this study, we synthesized derivatives based on the structure of **1x** with the benzimidazole scaffold and explored their antiresorptive potential. In total, 61 compounds containing either benzimidazole-2-substituted phenyl or pyridine propyl ketenes were synthesized. The compounds were evaluated for their potential to inhibit the kinase activity of Cat K. Many derivatives with benzimidazole scaffold showed inhibitory activity at less than 10 μM against Cat K *in vitro*. Then, we tested the selectivity of **1x**, **A20**, **A22**, and **A32** (Table 1) against several other cathepsins (L, S and B) and found that these compounds were highly selective for Cat K. Modelling studies identified several favourable interactions of **A22** with the active pocket of Cat K. Surface plasmon resonance (SPR) analysis confirmed the high affinity of **A22** to Cat K. Compounds **A20**, **A22** and **A32** showed inhibitory activity toward OCs and also inhibited bone resorption caused by C-telopeptide (CTX-I) decrease observed *in vitro*. Moreover, **A22** also increased spinal bone density in zebrafish.

2. Results and discussion

2.1 Chemistry

The search for potential Cat K inhibitors led to the identification of compound **1x** with a scaffold containing benzimidazole, a carbonyl group, and a double bond that is required for *in vitro* Cat K inhibition. The design and synthesis of a series of **1x** derivatives were performed as follows. The synthesis route of benzimidazole-2-substituted phenyl or pyridine propyl ketenes is described in Scheme 1. In total, 61 derivatives have been synthesized. There are different substituents on the two aromatic rings. In this round of synthesis, we only implanted substituents with smaller size, such as methyl, halogen or cyano groups. The detailed structures of the compounds are reported in Table 1.

2.2 Inhibition of Cat K *in vitro* and preliminary structure–activity relationships

The inhibitory activities of our focused compound library against Cat K are reported in Table 1 including odanacatib, which was used as a positive control. Importantly, many derivatives of scaffold A showed Cat K inhibitory effects at concentrations below 100 μM, which confirmed that this novel scaffold has a high potential to serve as a template for antiresorptive agents.

The phenyl or pyridine substitution (such as **A4** and **A39**) in the scaffold is favoured. The 2-substitution on the phenyl ring seems detrimental to Cat K inhibitory activities according to the IC_{50} data (>100 μM) of **A11**, **A15**, **A27**, and **A30**. The

Table 1 *In vitro* inhibitory activities (IC_{50}, μM) of compounds with scaffold A against Cat K

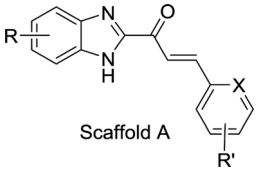

Scaffold A

Compd.	X	R	R′	IC_{50}	Compd.	X	R	R′	IC_{50}
A1	N	H	3′-Cl	26.15	**A33**	C	5-Cl	4′-CN	2.61
A2	N	H	4′-Cl	2.47	**A34**	C	4-Cl	3′-CN	6.19
A3	N	H	5′-Cl	8.48	**A35**	N	5,6-Dichloro	H	6.94
A4	N	H	6′-Cl	8.83	**A36**	C	5,6-Dichloro	3′-CN	7.62
A5	N	H	3′-Me	9.51	**A37**	C	5,6-Dichloro	4′-CN	5.57
A6	N	H	6′-Me	28.14	**A38**	N	5-Br	H	7.34
A7	N	H	5′-Br	6.12	**A39**	C	5-Br	3′-Cl	6.67
A8	N	H	6′-Br	9.48	**A40**	C	5-Br	3′-CN	2.34
A9	N	H	3′-F	3.75	**A41**	C	5-Br	4′-CN	0.77
A10	N	H	6′-OMe	8.96	**A42**	N	5-NO_2	H	6.54
A11	C	H	2′-CN	>100	**A43**	C	5-NO_2	H	8.19
A12	C	H	3′-CN	7.33	**A44**	C	5-NO_2	2′-Cl	11.01
A13	C	H	4′-CN	9.16	**A45**	C	5-NO_2	3′-Cl	10.70
A14	N	5-Me	H	25.86	**A46**	C	5-NO_2	4′-Cl	26.11
A15	C	5-Me	2′-CN	>100	**A47**	C	5-NO_2	2′-Br	11.32
A16	C	5-Me	3′-CN	47.04	**A48**	C	5-NO_2	3′-Br	9.70
A17	C	5-Me	4′-CN	2.96	**A49**	C	5-NO_2	4′-Br	15.90
A18	N	5-Cl	H	4.24	**A50**	C	5-NO_2	3′-Me	25.41
A19	N	5-Cl	3′-Cl	7.89	**A51**	C	5-NO_2	3′-CN	3.14
A20	N	5-Cl	4′-Cl	0.60	**A52**	C	5-NO_2	3′-OMe	22.91
A21	N	5-Cl	5′-Cl	4.73	**A53**	N	5-NH_2	H	4.29
A22	N	5-Cl	6′-Cl	0.44	**A54**	C	5-NH_2	H	8.75
A23	N	5-Cl	3′-Me	15.49	**A55**	C	5-NH_2	2′-Cl	9.09
A24	N	5-Cl	5′-Br	5.26	**A56**	C	5-NH_2	3′-Cl	4.38
A25	N	5-Cl	3′-F	2.82	**A57**	C	5-NH_2	4′-Cl	6.40
A26	N	5-Cl	6′-OMe	6.07	**A58**	C	5-NH_2	2′-Br	18.77
A27	C	5-Cl	2′-Cl	>100	**A59**	C	5-NH_2	3′-Br	4.11
A28	C	5-Cl	3′-Cl	23.42	**A60**	C	5-NH_2	4′-Br	4.99
A29	C	5-Cl	3′-Br	3.06	**A61**	C	5-NH_2	3′-Me	9.39
A30	C	5-Cl	3′-OMe	>100	**1x**	N	H	H	10.04
A31	C	5-Cl	2′-CN	51.14	Odanacatib				0.002
A32	C	5-Cl	3′-CN	0.88					

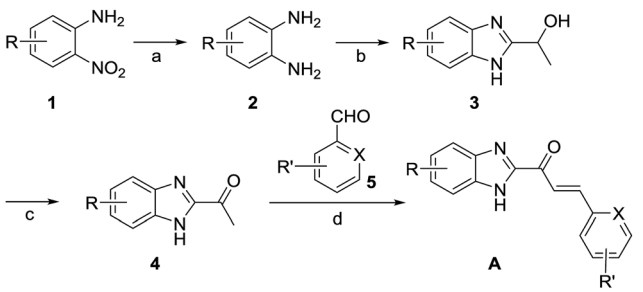

Scheme 1 Synthesis route of derivatives of **1x** started from **1** or **2**. (a) H_2, Pd/C, 30 °C; (b) 2-hydroxypropanoic acid, 4 M HCl, H_2O, 90 °C; ammonia; (c) TEMPO, NaClO, KBr, CH_3CN, r.t.; (d) NaOH, CH_3CH_2OH, r.t.

5-halogen substitution on benzimidazole appears to be favourable for the activity. **A20**, **A22**, **A32**, and **A41** showed inhibitory activities below 1 μM. Halogen and cyano group substitution on the terminal phenyl or pyridine ring may also contribute to the activity. The molecular docking calculations of **A22** (Cat K IC_{50} = 0.44 μM, Fig. 4) in the Cat K active pocket also suggested that its imidazole H atom formed a hydrogen bond with the O atom of the backbone carbonyl group at N161. This could explain why compounds benzoxazole **1o** and benzothiazole **1p** did not show any Cat K inhibiting effect. They lack this key hydrogen bond donor in their scaffold which appears to be a necessity for this activity. The phenyl ring of benzimidazole was coplanar with the glycine shelf (G23) and generated a hydrophobic interaction. The hydrophobic interaction between benzimidazole and C25 also enhanced the affinity of **A22** and Cat K. Thus, chlorine substitution on benzimidazole of **A22** is beneficial to the affinity to Cat K.

2.3 Selectivity of the inhibition of cathepsins *in vitro*

We compared the inhibitory activities of compounds **1x**, **A20**, **A22**, and **A32** against Cat K, Cat L, Cat S, and Cat B (Table 2).

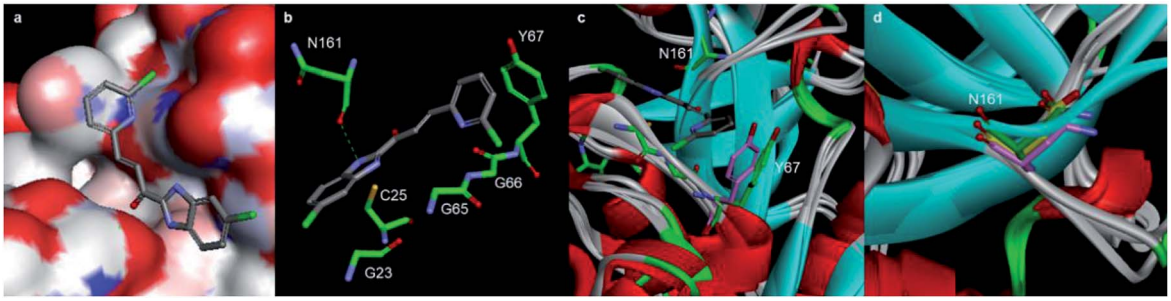

Fig. 4 Molecular docking calculations of the binding mode of **A22** with Cat K (PDB code: 4dmy). (a) and (b) The calculated interactions of **A22** (grey) with amino acids (green) in the active pocket of Cat K. (c) Overlay of the crystal structures of Cat L (PDB code: 6ezp), Cat S (PDB code: 4bs5) and Cat B (PDB code: 6ay2) with Cat K. N161 (green) of Cat K located at a loop region where the conformations of the Cat L, S, B and K are different. Compared to the orientation of Y193 (purple) of Cat S, Y67 (green) of Cat K has much less clash with pyridine ring of **A22**. (d) Backbone carbonyl groups of N161 of Cat K, N286 (purple) of Cat S and D162 (yellow) of Cat L.

Table 2 Inhibitory activity against Cat K, Cat L, Cat S and Cat B *in vitro*

	IC_{50} (μM)			
Compd.	Cat K	Cat L	Cat S	Cat B
1x	10.04	15.82	>100	>100
A20	0.60	1.64	24.73	47.73
A22	0.44	2.62	46.72	73.85
A32	0.88	1.79	25.34	101.76
Odanacatib	0.002	8.46	0.013	0.013

Compounds **1x**, **A20**, **A22**, and **A32** showed an inhibitory effects against the cathepsins, especially toward Cat K and Cat L. The order of the inhibitory activities of the four test compounds against the cathepsins were Cat K > Cat L > Cat S > Cat B. The selectivity of **A22** for Cat K over Cat S and Cat B was 106 and 168 times, respectively. According to the docking result, the hydrogen bond between **A22** and N161 of Cat K probably played a key role of the selectivity of **A22**. N161 of Cat K was in a loop region where the conformation of Cat B was highly different from Cat L, S, and K (Fig. 4c). Different from the loops of Cat K, L and S, it was a β-sheet of Cat B in this region. There was no asparagine here in Cat B. The change of asparagine to histidine and glycine distorted the binding pocket, which explained well that **A22** showed much weaker inhibitory activity against Cat B. Similar to their counterpart N161 in Cat K, D162 of Cat L and N286 of Cat S (Fig. 4d) also can form hydrogen bond with **A22**. **A22** showed high inhibiting effect against Cat L. But the higher clash of Y193 of Cat S to **A22** may alleviate the interaction (Fig. 4c).

As compared to the inhibitory activities of **1x**, the positive control odanacatib had a higher activity against Cat K and Cat L, but a lower activity against Cat S and Cat B. The selectivity of odanacatib for Cat K over Cat S and Cat B was 6.5 times for both enzymes. The order of the inhibitory activity of odanacatib against the cathepsins was Cat K > Cat S = Cat B > Cat L. These results indicated that **A22** and odanacatib differed in their selectivity toward cathepsin family proteins and, therefore, may differ in their activity and toxicity. Therefore, **A22** has the potential to be novel antiresorptive agents.

2.4 Antiresorptive effects *in vitro*

Type I collagen comprises about 95% of the entire collagen content of bone.[28] During skeletal renewal, type I collagen is degraded, releasing short peptide fragments into the bloodstream. The bone resorption process can be studied *in vitro* by culturing bone cells on bone sections or dentin sheets. During the process of bone resorption by OCs, the type I collagen C-terminal peptide (CTX-I) is degraded into fragments and released. In this experiment, the concentration of CTX-I released into the cell culture medium by bone degradation can be detected and quantified by ELISA. The *in vitro* antiresorptive effect of our compounds was tested in RANKL-induced RAW264.7 cells. Osteoclastic features can be induced in RAW264.7 by RANKL with high efficiency and reproducibility.[29] We detected the CTX-I[26,30,31] concentration released into the culture medium from RANKL-induced RAW264.7 cells by ELISA.

Importantly, RAW264.7 cells released much less CTX-I in the presence of A20, A22, A32, 1×, and positive control odanacatib, as compared to that released by untreated RAW264.7 cells. The concentrations of all experimental compounds and positive control drugs were 5 μM. The antiresorptive effects of all the experimental compounds was similar to that of odanacatib, especially the activity of **A20** was much stronger than that of the control drug. And also the efficacy of all the test compounds was significantly better than that of **1x** on RAW264.7 cells (Fig. 5A).

2.5 Inhibition of osteoclast (OC) cells

The inhibition of OCs *in vitro* was tested by counting the numbers of tartrate-resistant acid phosphatase (TRAP) positive cells. In this experiment, the RANKL-induced RAW264.7 cells were identified by OC-specific TRAP staining specific. The RANKL-induced RAW264.7 cells were incubated with the test compounds added at 20 μg mL^{-1}. After 72 h of culture, the TRAP staining was performed and the TRAP + cells were counted. As compared to the growth of the untreated control OCs, the growth of the OCs incubated with the test compounds (20 μg mL^{-1}) was reduced. The OC growth inhibition of A20, A22, and A32 was 31.3%, 33.3%, and 42.2%, respectively (Fig. 5B).

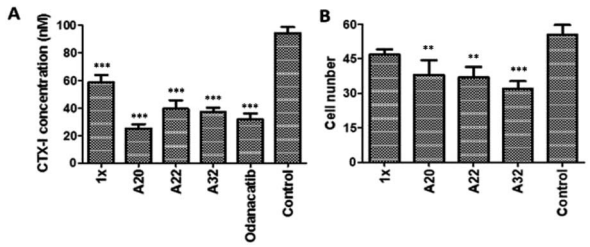

Fig. 5 (A) CTX-I detection of test compounds in the bone absorption process; (B) Effects on OC differentiation by test compounds *in vitro*. Three replicates were tested in each group. **Differences from the control group with probability $p < 0.05$. ***Differences from the control group with probability $p < 0.001$. The p value is calculated by Tukey–Kramer multiple comparisons test. The difference is considered statistically significant when probability p value is less than 0.05 and statistically highly significant when probability p value is less than 0.001.

2.6 Binding affinity to Cat K tested by SPR

To determine whether the active compounds can bind to Cat K, real-time binding analysis by SPR (Biacore 8K) was performed using Cat K and different dilutions of **A20** and **A22** (Fig. 6). The two compounds showed moderately strong affinities to Cat K. The calculated affinities (KD) of **A20** and **A22** to Cat K were 53.2 ± 43.7 μM and 17.2 ± 5.6 μM, respectively. Moderately strong affinities implied that the compounds may show antiresorptive efficacy *in vivo via* inhibition of Cat K.

2.7 OP therapeutic activity in zebrafish

To probe into the *in vivo* activities, we chose **A22** as a pilot compound and evaluated its activity in zebrafish[32,33] because **A22** was the most potent Cat K inhibitor *in vitro* among our focused library compounds and showed high selectivity and affinity to Cat K. Etidronate disodium was used as a positive control drug. Etidronate disodium is a bone resorption inhibitor and now mainly used as an antiosteoporotic medication.[34] Its action mechanism involves the hydroxyapatite crystal growth inhibition according to the *in vitro* chemisorption onto the crystal surface.[35] Prednisone is a glucocorticoid medication and often used to suppress the immune system and relieve inflammation. The use of prednisone can induce bone loss.[36–38] In our study, we use prednisone to set up a zebrafish bone loss model.

Our dosing pilot study showed at the concentration of 1.00 μM, **A22** didn't show obvious toxicity to the 30 zerafish in the group. We then tested OP therapeutic activity in zebrafish of A22 at concentrations of 0.11, 0.33, and 1.00 μM. Fluorescent chromophore calcein, which binds specifically to calcified skeletal structures, was used to indicate zebrafish spine bone density.[39] Fluorescence intensities were enhanced as compared to that of the model group, indicating that **A22** treatment improved bone density at tested concentrations. **A22** also showed dose–response relationship in OP zebrafish. At the highest concentration group, **A22** exhibited higher activity than etidronate disodium (ED) (Fig. 7). The OP therapeutic effect in zebrafish bone loss model showed that **A22** is a promising anti-OP agent.

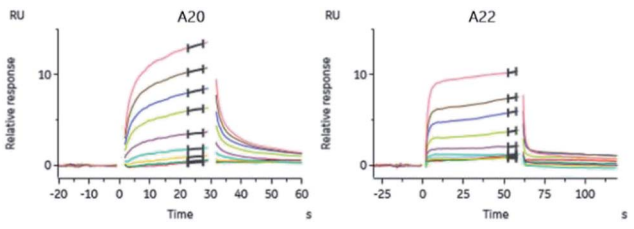

Fig. 6 Binding curves of **A20** and **A22** dilutions. The affinities (KD) were calibrated with the steady state affinity 1 : 1 binding model using the evaluation software of Biacore 8K.

3. Experimental section

3.1 Chemistry

3.1.1 General information. All reagents and solvents were purchased and used without further purification unless specified. The ^{1}H NMR and ^{13}C NMR spectra were recorded with a Bruker BioSpin GmbH spectrometer (400 MHz) in d_6-DMSO and the internal solvent residual peaks were used as references. The high-resolution mass spectra (HRMS) were recorded on a Thermo Scientific LTQ Orbitrap XL with an ESI mass selective detector. The melting points (mp) were determined using Mettler Toledo MP 90. Flash column chromatography using a silica gel (200–300 mesh) purchased from Qingdao Haiyang Chemical Co. Ltd was performed on a Combiflash RF200.

3.1.2 Synthesis of A22. To a 250 mL three-necked round bottom bottle, 4-chlorobenzene-1,2-diamine (**2**, 7.13 g, 0.05 mol) and 85% 2-hydroxypropanoic acid (7.95 g, 0.075 mol) were added and mixed with 40 mL of 4 mol L^{-1} HCl. The mixture was heated to 90 °C and stirred for 5 h. After the full conversion of the starting material (as monitored by TLC), the reaction was cooled to 30 °C. The pH of the mixture was adjusted to 8 using ammonia water. A white precipitate formed that was collected by filtration, washed with water, and dried under air in a culture dish followed by a drying step performed under vacuum in an oven. A product with the designation 1-(5-chloro-1*H*-benzo[*d*] imidazo l-2-yl)ethan-1-ol was obtained as a white solid (3, yield 93%), MS (ESI) *m*/*z*: 197 $[M + H]^+$

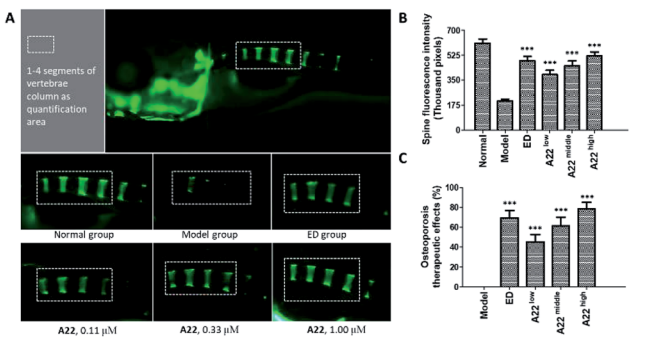

Fig. 7 Therapeutic effect of **A22** in OP zebrafish. (A) Zebrafish spine fluorescence intensity data were collected within the white rectangle area. **A22** was administered at a dose of 0.11 μM, 0.33 μM, 1.00 μM, and etidronate disodium (ED) was administered at a dose of 600 μM; (B) spine fluorescence intensity data were calculated based on values obtained from 30 fish each group. (C) **A22** therapeutic effect on zebrafish OP. ***Differences from the model group with probability $p < 0.001$. The p value is calculated using Dunnett's T test and differences with probability $p < 0.05$ are considered statistically significant.

1-(5-Chloro-1*H*-benzo[*d*]imidazol-2-yl)ethan-1-ol (**3**, 1.97 g, 0.01 mol), TEMPO (0.016 g, 0.1 mmol) and KBr (0.12 g, 1 mmol) were added to a 100 mL three-necked round bottom bottle. Then, 20 mL of acetrile and 20 mL of water were added. An 8% aqueous sodium hypochlorite (13.96 g, 0.015 mol) solution was added dropwise within 20 min while keeping the temperature of the mixture between 10 °C and 15 °C. The mixture was stirred for 30 min until full conversion (as monitored by TLC). The mixture was extracted by ethyl acetate (50 mL × 3). The organic phases were combined and washed with 60 mL of 10% sodium thiosulfate and 60 mL of brine. The organic layer was then separated, dried over anhydrous Na_2SO_4 and evaporated to recover 1-(5-chloro-1*H*-benzo[*d*]imidazol-2-yl)ethan-1-one (4, yield 71%). mp 156.1–157.4 °C; MS (ESI) *m*/*z*: 195 $[M + H]^+$.

1-(5-Chloro-1*H*-benzo[*d*]imidazol-2-yl)ethan-1-one (**4**, 607.2 mg, 3.1 mmol) and ethanol (10 mL) were added to a 25 mL three-necked round bottom bottle. The resulting mixture was stirred until 4 was fully dissolved. NaOH (0.12 g, 3.12 mmol) was then added and then stirred for another 15 min. 6-Chloropicolinaldehyde (0.44 g, 3.12 mmol) was added. The reaction was stirred for 2 h until full conversion (as monitored by TLC). The reaction was quenched with 5 mL of water while stirring. A yellow solid precipitated from the solution. Filtration was performed to collect the solid and wash it with water. The solid was first dried under air in a culture dish and then separated by flash column chromatography (PE : EA = 10 : 1). (*E*)-1-(5-chloro-1*H*-benzo[*d*]imidazol-2-yl)-3-(6-chloropyridin-2-yl)prop-2-en-1-one (**A22**, yield 54%) was obtained as yellow solid. mp 251.4–252.7 °C; ^{1}H NMR (400 MHz, d6-DMSO) δ 13.68 (s, 1H), 8.39 (d, J = 15.7 Hz, 1H), 7.99–7.93 (m, 2H), 7.88 (d, J = 15.7 Hz, 1H), 7.84 (d, J = 7.5 Hz, 1H), 7.58 (d, J = 7.6 Hz, 2H), 7.43–7.34 (m, 1H); ^{13}C NMR (101 MHz, d_6-DMSO) δ 181.26, 153.43, 151.18, 141.46, 134.07, 130.78, 126.19, 125.80, 124.38, 123.28, 121.01, 114.84, 112.88; HRMS calcd for $C_{15}H_{10}ON_3Cl_2^+$ $[M + H]^+$ 318.01954, found 318.01942.

3.1.3 Syntheses of A1–A21 and A23–A61. The syntheses of **A1–A21** and **A23–A61** used the protocol described for the synthesis of **A22** and illustrated in Scheme 1. The starting materials differed. Specifically, the syntheses of **A1–A13**, **A14–A17**, **A18–A33**, **A34**, **A35–A37**, **A38–A41**, and **A42–A61** were started from benzene-1, 2-diamine, 4-methylbenzene-1, 2-diamine, 4-chlorobenzene-1, 2-diamine, 4-chlorobenzene-1,2-diamine, 2-chloro-6-nitroaniline, 5-chloro-2-nitroaniline, 4-bromobenzene-1, 2-diamine and 4-nitrobenzene-1, 2-diamine, respectively. The data for the characterization of these compounds are provided in the ESI.†

3.2 Molecular docking calculations

CDOCKER of Discovery Studio 4.5 was used to carry out the docking simulation of the compounds to the protein. X-ray crystal structure of Cat K (PDB code 4dmy) was used for the docking studies. The ligand was extracted from the catalytic active site of Cat K, which was defined as the docking site for binding. Both the receptor and the compounds were employed using the CHARMm force field before docking. A higher CDOCKER score (*i.e.* –DOCKER _ENERGY) indicates a more favourable affinity. Using the docking calculations of CDOCKER, we also obtained the exact pose of the ligand in 4dmy.

3.3 Enzymatic activity assays *in vitro*

Quenched fluorescent resonance energy transfer (QFRET) technology was used to test the inhibitory activity of the compounds against Cat K (ENZO BML-SE553) catalysing the cleavage of the synthetic peptide Z-Phe-Arg-AMC. Compounds were tested at eight concentrations (diluted from 200 μg mL^{-1}, three replicates per dilution). To each test sample well on a 96-well plate, 2 μL of test compound were mixed with 25 μL of Cat K (0.3 ng mL^{-1}). In control wells, DMSO was added instead of the compounds. In blank wells, DMSO was added instead of compounds and buffer was added instead of Cat K solution. The plate was incubated for 15 min at 37 °C. The fluorescence (F1) was determined at a wavelength of 355 nm excitation and 460 nm emission. Then, 25 μL of 20 μM of Z-Phe-Arg-AMC was then added and the plate was incubated for 1 h at 37 °C. Then, the fluorescence (F2) was measured again at a wavelength of 355 nm excitation and 460 nm emission. The calculation was performed as follows: inhibition (%) = [control (F2–F1) − sample (F2–F1)]/[control (F2–F1) − blank (F2–F1)] × 100%. IC_{50} was calculated using SPSS.

The Cat L (Sigma, C6854), Cat S (Sigma, SRP6297), and Cat B (Sigma, C8571) inhibitory assays were carried out using a similar protocol, except that the substrates for Cat S and Cat B were replaced with Ac-Lys-Gln-Lys-Leu-Arg-AMC and Z-Arg-Arg-AMC, respectively.

3.4 The inhibition of TRAP in RANKL-induced OC

RAW264.7 cells were seeded into a sterile 96-well plate at a density of 1 × 102 cells per well. To the DMEM culture medium, 10 ng mL^{-1} RANKL was added to induce the differentiation in RAW264.7 cells. Test compounds were added at 20 μg mL^{-1}; each compound was tested in triplicate. Wells without a compound were used as blanks. The cells were incubated for 72 h at 37 °C in 5% CO_2. Then, the culture medium was removed. The residues in the wells were fixed with fixative solution (25.5% citrate solution + 66.3% acetone + 8.2% of 37% formaldehyde) for 30 s and washed with deionized water. Then mixing solution (naphthol AS-BI phosphate solution and tartrate solution) was added and the plate was incubated at 37 °C in the dark. After a final washing step with deionized water, the TRAP-positive cells were counted.

3.5 CTX-I concentration

RAW264.7 cells were seeded into a sterile 12-well plates with bovine femur slices at a density of 1 × 105 cells per well. To the DMEM culture medium, 50 ng mL^{-1} RANKL was added to induce the differentiation in RAW264.7 cells. Test compounds were added at a concentration of 5 μM. The cells were cultured for five days at 37 °C under 5% CO_2. The culture supernatants were collected by centrifugation for analysing the CTX-I concentrations by ELISA.

3.6 Real-time binding to Cat K and analysed by SPR

SPR experiments were carried out using a Biacore 8K (GE Healthcare) at 25 °C. Cat K (ENZO BML-SE553) was preconditioned in pH 5.0 sodium acetate and then immobilized to a CM7 chip by amine coupling. Running buffer was 50 mM NaOAc (pH 5.5), 0.01% P20, 2 mM EDTA, 100 μM DTT. When the affinities of compounds were tested, 5% DMSO was added. Ten concentrations of each compound were used. **A20** was diluted from 100 μM by two-fold serial dilution. **A22** was diluted from 50 μM by two-fold serial dilution. Compounds were injected to the surface of the protein-coupled chip channels at the flow rate of 30 μL min^{-1}. The affinities (K_D) were calibrated with the steady state affinity 1 : 1 binding model with the evaluation software of Biacore 8K. The affinities of **A20** and **A22** were tested twice and five times, respectively.

3.7 OP therapeutic effects in zebrafish B

OP was induced in zebrafish at the age of 2 dpf (day-post-fertilization) by treating normal wild-type AB zebrafish with prednisone for 96 h. Zebrafish larvae were randomly added to wells in 6-well plates. There were 30 fish per well. Etidronate disodium and different concentrations of **A22** were dissolved by water and then added to different wells to target concentration. The zebrafish larvae were incubated with the compounds for 96 h at 28 °C.

Zebrafish larvae aged at 7 dpf was dyed with 0.05% calcein solution for 15 min. Then it was washed with water for 15 min on the shaking table (repeated three times). The zebrafish larvae were fixed with methyl cellulose. The spine fluorescent intensity (SFI) images of the calcein-stained vertebrate column were captured with AZ100 fluorescence microscopy (Nikon). The integral optical density of 1 to 4 segments of vertebrae was measured by Image *J* analysis software. OP therapeutic effects (%) = (sample SFI − model SFI)/(normal SFI − model SFI) × 100%.

All animal procedures were performed in accordance with the Guidelines for Care and Use of Laboratory Animals of Institute of Medicinal Biotechnology, Chinese Academy of Medical Science and Peking Union Medical College and approved by the Animal Ethics Committee of Institute of Medicinal Biotechnology.

4. Conclusions

In this study, a total of 61 derivatives were designed and synthesized with a shared scaffold that has not been reported elsewhere as Cat K inhibitors and anti-osteoporosis agents. Several derivatives showed an IC_{50} value below 10 μM against Cat K. We rigorously analysed the structure–activity relationship. **A20**, **A22**, and **A32** had a significantly higher inhibitory activity against Cat K *in vitro* than that of the lead compound **1x**. Real-time binding analysis by SPR and molecular docking calculations confirmed the binding of **A22** to Cat K *in vitro*. **A22** improved spinal bone density in zebrafish with induced OP at an efficacy that was higher than that of the marketed therapeutic bone metabolizer etidronate disodium. Hence, we believe that **A22** represents a novel lead compound for anti-resorptive drugs that will be examined for further improvements in structure-based drug design, therapeutic efficacy, and pharmacokinetics.

Conflicts of interest

There are no conflicts to declare.

Acknowledgements

We gratefully acknowledge the grants from the CAMS Innovation Fund for Medical Sciences (CIFMS, 2017-I2M-3-019) and the National Natural Science Foundation of China (81473097, 81402800).

Notes and references

1 S. Tanaka, *Am. J. Nephrol.*, 2007, **27**, 466–478.
2 E. Hernlund, A. Svedbom, M. Ivergard, J. Compston, C. Cooper, J. Stenmark, E. V. McCloskey, B. Jönsson and J. A. Kanis, *Arch. Osteoporos.*, 2013, **8**, 1–115.
3 O. Ström, F. Borgström and J. A. Kanis, *Arch. Osteoporos.*, 2011, **6**, 59–155.
4 Z. Amso, J. Cornish and M. A. Brimble, *Med. Res. Rev.*, 2016, **36**, 579–640.
5 S. Fujiwara, E. Hamaya, M. Sato, P. Graham-Clarke, J. A. Flynn and R. Burge, *Clin. Interventions Aging*, 2014, **5**, 1879–1893.
6 B. R. Bhavnani and F. Z. Stanczyk, *J. Steroid Biochem. Mol. Biol.*, 2014, **142**, 16–29.
7 S. Sanders and S. A. Geraci, *South. Med. J.*, 2013, **106**, 698–706.
8 G. Mazziotti, J. Bilezikian, E. Canalis, D. Cocchi and A. Giustina, *Endocrine*, 2012, **41**, 58–69.
9 J. A. Kanis, E. V. McCloskey, H. Johansson, A. Oden, L. J. Melton and N. Khaltaev, *Bone*, 2008, **42**, 467–475.
10 A. G. Costa, N. E. Cusano, B. C. Silva, S. Cremers and J. P. Bilezikian, *Nat. Rev. Rheumatol.*, 2011, **7**, 447–456.
11 M. Novinec and B. Lenarčič, *Biol. Chem.*, 2013, **394**, 1163–1179.
12 M. Gowen, F. Lazner, R. Dodds, R. Kapadia, J. Field, M. Tavaria, I. Bertoncello, F. Drake, S. Zavarselk, I. Tellis, P. Hertzog, C. Debouck and I. Kola, *J. Bone Miner. Res.*, 1999, **14**, 1654–1663.
13 M. T. Drake, B. L. Clarke, M. J. Oursler and S. Khosla, *Endocr. Rev.*, 2017, **38**, 325–350.
14 J. Wijkmans and J. Gossen, *Expert Opin. Ther. Pat.*, 2011, **21**, 1611–1629.
15 M. Frizler, M. Stirnberg, M. T. Sisay and M. Gütschow, *Curr. Top. Med. Chem.*, 2010, **10**, 294–322.
16 J. Y. Gauthier, N. Chauret, W. Cromlish, S. Desmarais, L. T. Duong, J. P. Falgueyret, D. B. Kimmel, S. Lamontagne, S. Léger, T. LeRiche, C. S. Li, F. Massé, D. J. McKay, D. A. Nicoll-Griffith, R. M. Oballa, J. T. Palmer, M. D. Percival, D. Riendeau, J. Robichaud, G. A. Rodan, S. B. Rodan, C. Seto, M. Thérien,

V. L. Truong, M. C. Venuti, G. Wesolowski, R. N. Young, R. Zamboni and W. C. Black, *Bioorg. Med. Chem. Lett.*, 2008, **18**, 923–928.

17 H. Xie, G. Chen and R. N. Young, *J. Med. Chem.*, 2017, **60**, 7012–7028.

18 S. Kumar, L. Dare, J. A. Vasko-Moser, I. E. James, S. M. Blake, D. J. Rickard, S. M. Hwang, T. Tomaszek, D. S. Yamashita, R. W. Marquis, H. Oh, J. U. Jeong, D. F. Veber, M. Gowen, M. W. Lark and G. Stroup, *Bone*, 2007, **40**, 122–131.

19 D. S. Yamashita, R. W. Marquis, R. Xie, S. D. Nidamarthy, H. J. Oh, J. U. Jeong, K. F. Erhard, K. W. Ward, T. J. Roethke, B. R. Smith, H. Y. Cheng, X. Geng, F. Lin, P. H. Offen, B. Wang, N. Nevins, M. S. Head, R. C. Haltiwanger, S. A. Narducci, L. M. Liable-Sands, B. Zhao, W. W. Smith, C. A. Janson, E. Gao, T. Tomaszek, M. McQueney, I. E. James, C. J. Gress, D. L. Zembryki, M. W. Lark and D. F. Veber, *J. Med. Chem.*, 2006, **49**, 1597–1612.

20 J. P. Falgueyret, S. Desmarais, R. Oballa, W. C. Black, W. Cromlish, K. Khougaz, S. Lamontagne, F. Massé, D. Riendeau, S. Toulmond and M. D. Percival, *J. Med. Chem.*, 2005, **48**, 7535–7543.

21 C. Jerome, M. Missbach and R. B. Gamse, *Osteoporosis Int.*, 2012, **23**, 339–349.

22 S. Nagase, M. Ohyama, Y. Hashimoto, M. Small, J. Sharpe, J. Manako, T. Kuwayama and S. Deacon, *J. Bone Miner. Metab.*, 2015, **33**, 93–100.

23 Y. Ochi, H. Yamada, H. Mori, Y. Nakanishi, S. Nishikawa, R. Kayasuga, N. Kawada, A. Kunishige, Y. Hashimoto, M. Tanaka, M. Sugitani and K. Kawabata, *Bone*, 2011, **49**, 1351–1356.

24 H. F. Guo, H. Y. Shao, Z. Y. Yang, S. T. Xue, X. Li, Z. Y. Liu, X. B. He, J. D. Jiang, Y. Q. Zhang, S. Y. Si and Z. R. Li, *J. Med. Chem.*, 2010, **53**, 1819–1829.

25 S. T. Xue, H. F. Guo, M. J. Liu, J. Jin, D. H. Ju, Z. Y. Liu and Z. R. Li, *Eur. J. Med. Chem.*, 2015, **96**, 151–161.

26 A. G. Dossetter, H. Beeley, J. Bowyer, C. R. Cook, J. J. Crawford, J. E. Finlayson, N. M. Heron, C. Heyes, A. J. Highton, J. A. Hudson, A. Jestel, P. W. Kenny, S. Krapp, S. Martin, P. A. MacFaul, T. M. McGuire, P. M. Gutierrez, A. D. Morley, J. J. Morris, K. M. Page, L. R. Ribeiro, H. Sawney, S. Steinbacher, C. Smith and M. Vickers, *J. Med. Chem.*, 2012, **55**, 6363–6374.

27 L. T. Wu, Z. Jiang, J. J. Shen, H. Yi, Y. C. Zhan, M. Q. Sha, Z. Wang, S. T. Xue and Z. R. Li, *Eur. J. Med. Chem.*, 2016, **114**, 328–336.

28 C. Niyibizi and D. R. Eyre, *Eur. J. Biochem.*, 1994, **224**, 943–950.

29 V. G. Palacios, L. J. Robinson, C. W. Borysenko, T. Lehmann, S. E. Kalla and H. C. Blair, *J. Biol. Chem.*, 2005, **280**, 13720–13727.

30 P. Garnero, M. Ferreras, M. A. Karsdal, R. Nicamhlaoibh, J. Risteli, O. Borel, P. Qvist, P. D. Delmas, N. T. Foged and J. M. Delaissé, *J. Bone Miner. Res.*, 2003, **18**, 859–867.

31 M. Herrmann and M. J. Seibel, *Clin. Chim. Acta*, 2008, **393**, 57–75.

32 A. Fleming, M. Sato and P. Goldsmith, *J. Biomol. Screening*, 2005, **10**, 823–831.

33 T. P. Barros, W. K. Alderton, H. M. Reynolds, A. G. Roach and S. Berghmans, *Br. J. Pharmacol.*, 2008, **154**, 1400–1413.

34 D. E. Padgett, K. G. Holley, M. Cummings, A. G. Rosenberg, D. R. Sumner, D. Conterato and J. O. Galante, *J. Arthroplasty.*, 2003, **18**, 677–686.

35 B. J. Thomas and H. C. Amstutz, *Hip*, 1987, 59–69.

36 F. N. Ton, S. C. Gunawardene, H. Lee and R. M. Neer, *J. Bone Miner. Res.*, 2005, **20**, 464–470.

37 L. Buckley and M. B. Humphrey, Glucocorticoid-Induced Osteoporosis, *N. Engl. J. Med.*, 2018, **379**, 2547–2556.

38 H. Wang, T. Feng, D. Guo, M. Zhang, L. Chen and Y. Zhou, *Molecules*, 2018, **23**, E2343.

39 S. J. Du, V. Frenkel, G. Kindschi and Y. Zohar, *Dev. Biol.*, 2001, **238**, 239–246.